Available online at www.sciencedirect.com
SCIENCE DIRECT®
Journal of Crystal Growth 283 (2005) 31–40
JOURNAL OF CRYSTAL GROWTH
www.elsevier.com/locate/jcrysgro

Three-dimensional microstructural characterization of GaN nonplanar substrate laterally epitaxially overgrown by metalorganic chemical vapor deposition

Wei Zhou[a,*], Dawei Ren[b], P.D. Dapkus[a,c]

[a]*Department of Materials Science, University of Southern California, Los Angeles, CA 90089, USA*
[b]*Department of Physics, University of Southern California, Los Angeles, CA 90089, USA*
[c]*Department of Electrical Engineering—Electrophysics, University of Southern California, Los Angeles, CA 90089, USA*

Received 14 March 2005; received in revised form 12 May 2005; accepted 19 May 2005
Available online 20 July 2005
Communicated by R. Bhat

Abstract

Transmission electron microscopy techniques are applied to investigate three-dimensional (3D) microstructures of the GaN nonplanar substrate selectively grown by metalorganic chemical vapor deposition. Two-step lateral epitaxial overgrowth (LEO) has been utilized and optimized to fabricate fully coalesced nonplanar mesa substrate templates with the trapezoidal cross-section. All threading dislocations (TDs) penetrating beyond the two adjacent mask windows are engineered to bend 90° in the lower TD bending layer after the first step of growth. The dislocations, which approach the GaN mesa top, are predominantly perfect **a** type dislocations with Burgers vectors of $\frac{1}{3}\langle 1\,1\,\bar{2}\,0\rangle$ and a density of $8\times10^{7}\,\mathrm{cm}^{-2}$, which is reduced by three orders of magnitude compared with that of bulk GaN. The spatial distribution of different types of dislocations in the LEO nonplanar substrate is demonstrated herein. The main sources of **a** type dislocations in the post-bending layer are byproducts of dislocation reactions occurring at the TD bending layer.

Keywords: A1. Dislocation reactions; A1. Dislocation reduction; A1. Threading dislocation; A1. Three-dimensional; A1. Transmission electron microscopy; A2. Two-step lateral epitaxial overgrowth

1. Introduction

GaN and its related alloys have the band gaps and optical characteristics suitable for such short wavelengths light sources as blue and ultra-violet light emitting diodes or lasers [1], which have commercial values in the applications of display,

*Corresponding author. Tel.: +3236207277; fax: +2137406022.
E-mail address: zhouw@usc.edu (W. Zhou).

0022-0248/$ - see front matter © 2005 Elsevier B.V. All rights reserved.
doi:10.1016/j.jcrysgro.2005.05.046

Report Documentation Page

Form Approved
OMB No. 0704-0188

1. REPORT DATE	2. REPORT TYPE	3. DATES COVERED
01 JUN 2005	**N/A**	**-**

4. TITLE AND SUBTITLE	5a. CONTRACT NUMBER
Three-dimensional microstructural characterization of GaN nonplanar substrate laterally epitaxially overgrown by metalorganic chemical vapor deposition	5b. GRANT NUMBER
	5c. PROGRAM ELEMENT NUMBER
6. AUTHOR(S)	5d. PROJECT NUMBER
	5e. TASK NUMBER
	5f. WORK UNIT NUMBER
7. PERFORMING ORGANIZATION NAME(S) AND ADDRESS(ES) **Department of Materials Science, University of Southern California, Los Angeles, CA 90089, USA**	8. PERFORMING ORGANIZATION REPORT NUMBER
9. SPONSORING/MONITORING AGENCY NAME(S) AND ADDRESS(ES)	10. SPONSOR/MONITOR'S ACRONYM(S)
	11. SPONSOR/MONITOR'S REPORT NUMBER(S)

12. DISTRIBUTION/AVAILABILITY STATEMENT
Approved for public release, distribution unlimited

13. SUPPLEMENTARY NOTES
See also ADM001923.

14. ABSTRACT

15. SUBJECT TERMS

16. SECURITY CLASSIFICATION OF:			17. LIMITATION OF ABSTRACT	18. NUMBER OF PAGES	19a. NAME OF RESPONSIBLE PERSON
a. REPORT	b. ABSTRACT	c. THIS PAGE			
unclassified	**unclassified**	**unclassified**	**UU**	**10**	

lighting, digital information storage and retrieval. In the context of role reversal, these material combinations are also candidates for ultra-violet photodetectors and solar blind detectors. The potential of III-nitride alloys for use in high-power and high-frequency transistors is also considerable due to the large carrier velocities, large total carrier concentrations in two-dimensional systems, large band discontinuities and high-junction-temperature tolerance [2,3].

However, there are many problems remaining to be solved, including the development of III-nitride substrates, the reduction of dislocation density and residual stresses. Growths of monocrystalline III-nitride boules from which wafers can be obtained have not been achieved [4]. Owing to the current need to grow on lattice-mismatched substrates, the typically epitaxially grown III-nitride materials are known to exhibit a high density of dislocations in the 10^9–$10^{10}\,cm^{-2}$ range [5], which deteriorate the optoelectronic and transport properties of GaN-based films [6,7]. For example, the threading dislocations (TDs) are conduits for charge breakdown of rectifying contacts, act as non-radiative recombination centers and reduce significantly the lifetime of laser diodes (LDs) [4]. Thus the reduction of dislocation density in the GaN crystals is necessary to improve the performance of LD devices [8].

Recently, lateral epitaxial overgrowth (LEO), where lateral epitaxy occurs over an amorphous SiO_2 or SiN_x mask, has been studied extensively as an approach to efficiently decrease the defect density of the GaN films grown on Al_2O_3 [9,10]. The densities in the GaN template layers are reported to be in the $10^8\,cm^{-2}$ range for **a**-type dislocations with Burgers vector $\mathbf{b} = \frac{1}{3}\langle 1\,1\,\bar{2}\,0\rangle$ and **a** + **c**-type dislocations with Burgers vector $\mathbf{b} = \frac{1}{3}\langle 1\,1\,\bar{2}\,3\rangle$, whereas the density of **c**-type dislocations with Burgers vector $\mathbf{b} = \langle 0\,0\,0\,1\rangle$can approach the $10^7\,cm^{-2}$ range at best [11]. Various advanced techniques, such as FIELO [12], FACE-LO [13], Pendeo–Epitaxy [14] and mass transport techniques [15], were contrived to obtain low-dislocation-density GaN crystal. Complicated microstructures, such as wing tilting, 90° bending of TDs, and generation of horizontal dislocations (HDs) have been reported in the GaN layers by the above techniques [16,17]. Most recently, two-step planar LEO has been reported to successfully lower the dislocation density to the $10^7\,cm^{-2}$ ranges in the lateral epitaxy area [18].

In our previous study [19], using nonplanar substrate templates as platforms to offer good optical confinement and current confinement has enabled successful fabrication of low threshold lasers in the InGaAs–GaAs system. A new approach based on a similar idea of nonplanar substrate templates is being studied in the InGaN–GaN system. Enhanced indium incorporation as well as the reduction of indium phase segregation has been achieved in the single InGaN quantum well grown on nonplanar LEO GaN grown by the two-step LEO technique [20].

The purpose of this article is to investigate, using transmission electron microscopy (TEM), the three-dimensional (3D) microstructures of nonplanar GaN substrates grown by our two-step LEO method. The experimental procedure is described in Section 2. The distributions of dislocation categories in different layers of the nonplanar substrates will be described in Section 3, based on the invisibility criterion (i.e., $\mathbf{g}*\mathbf{b} = 0$). A discussion of dislocation behaviors in the nonplanar substrate templates will be presented thereafter. We use the classifications of **a, c** and **a** + **c** types here instead of "edge dislocation", "screw dislocation" and "mixed dislocation" because the edge and screw nature of the dislocation changes after bending but the Burgers vector is unchanged.

2. Experimental procedure

The metalorganic chemical vapor deposition (MOCVD) growth of GaN was performed in a Thomas Swan vertical reactor under the growth pressure of 200 Torr. Hydrogen was used as the carrier gas, while trimethylgallium and pure ammonia (NH_3) were used as the III and V column sources, if not designated otherwise. A 2-μm-thick GaN buffer layer was first deposited onto a c-Al_2O_3 (0 0 0 1) substrate with a conventional two-step process [21]. For the LEO growth, a 100-nm-thick stripe-patterned mask of SiN_x was fabricated on the buffer layer by plasma enhanced

CVD followed with a conventional photolithography and CF_4 reactive ion etching method. The stripe edges were parallel to the $[1\bar{1}00]$ direction of GaN, because it has been demonstrated that the lateral growth rate will be higher when the stripes are aligned along such a direction [22,23]. Subsequently, GaN nonplanar substrate templates were manufactured by MOCVD two-step LEO method, in which vertical growth was enhanced in the 1st step but lateral overgrowth would be favored in the 2nd step. In the first step, the growth rate of the inclined $\{11\bar{2}2\}$ facets is much slower than the (0001) facet so that the top c planes of two submesas will diminish and completely disappear with only $\{11\bar{2}2\}$ facets left. During the second step LEO, on the contrary, the growth rate of $\{11\bar{2}2\}$ facets will be increased much relative to that of the (0001) facet, until a smooth coalescence is achieved [20]. The detailed procedures for two-step LEO were presented elsewhere [24].

Cross-sectional and plan-view TEM samples were prepared by mechanical tripod polishing [25] combined with conventional Ar^+-ion milling. The TEM observation was carried out with either a Philips EM420 operating at 120 kV or an Akashi 002B operating at 200 kV. Some of the images are collaged from several photographs so as to gain better knowledge of the defect behavior over a large area.

3. Results and discussion

3.1. 3D view of GaN nonplanar substrate

The bright-field TEM images in Fig. 1 display typical 2D views of the microstructures inside the GaN nonplanar substrate, with different TEM view directions indicated in Fig. 1(a). Fig. 1(b) is a collaged TEM photo of its typical $(1\bar{1}00)$ transversal cross-section under the $[1\bar{1}00]$ zone axis. The LEO nonplanar GaN substrate has a trapezoidal cross-section with smooth (0001) and $\{11\bar{2}2\}$ facets. TDs in the buffer layer are stopped from propagating upwards by the SiN_x masks. Significantly, TDs through the mask opening will only thread up for around 8.2 μm before they all bend 90° towards the inclined $\{11\bar{2}2\}$ facets. This phenomenon of TD 90° bending was attributed to the dynamic stress field relaxation during the 1st step LEO growth, explained by the image force theory [26]. Therefore, the epitaxial layer can be divided into two sub-layers: one is the TD bending layer, referred to as the lower epitaxial layer containing all the bent TDs above the SiN_x masks; the other is the post-bending layer, as the upper layer that extends from the top of TD bending layer to the mesa top surface. Many HD segments, which exist in the wing area of the TD bending layer, are actually branches of bent-over TDs and aligned along $\langle 11\bar{2}0\rangle$ directions. Although all the TDs are stopped from entering the post-bending layer after bending, there are small remnant dislocations (RDs) in the post-bending layer mainly residing in and between two mask windows. The dislocation density of the post-bending layer is abruptly decreased to $\sim 8\times 10^7\,cm^{-2}$.

To understand the behavior of coalescence misfit dislocations better, the $(11\bar{2}0)$ cross-section of GaN nonplanar substrate is cut precisely through the center coalescence void line. While lapping the stripes parallel to the stripe direction of $[1\bar{1}00]$ with a tripod polisher, extremely precise control of the lapping stop position and polishing angles is realized for the first time to obtain a longitudinal cross-section sample right along the stripe center. A typical TEM image of this longitudinal cross-section is displayed under the $[11\bar{2}0]$ zone axis in Fig. 1(c), with the void trace indicated by a pair of arrows. Apparently, a major number of dislocations are contained in the TD bending layer and are even tangled into dislocation clusters. When entering the post-bending layer, the dislocation density decreases significantly. Observations in plan view enable us to obtain complementary views of the dislocation distribution in the nonplanar mesa from the top. Fig. 1(d) and (e), which are bright field images along the [0001] zone axis, show the top most region of the mesa. Dislocations are observed to be mostly edge-on or have short sections, and distribute randomly over the mesa surface. No coalescence line formed by dislocations is observed on the surface.

Fig. 2 is another $(11\bar{2}0)$ cross-sectional epilayer without the interference of bending contours, since it broke off from the SiN_x mask in the same

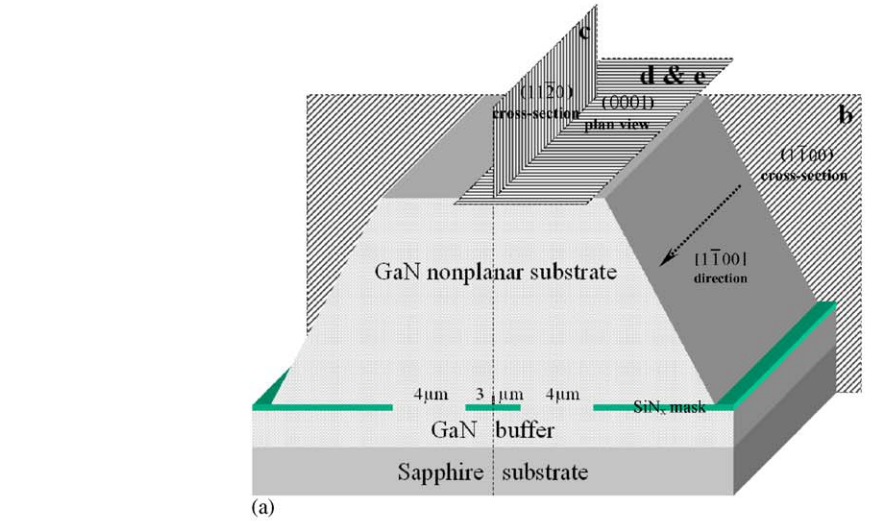
c
d & e
(11$\bar{2}$0)
cross-section
(0001)
plan view
b
(1$\bar{1}$00)
cross-section
GaN nonplanar substrate
[1$\bar{1}$00]
direction
4μm
3 μm
4μm
SiNx mask
GaN buffer
Sapphire substrate

(a)

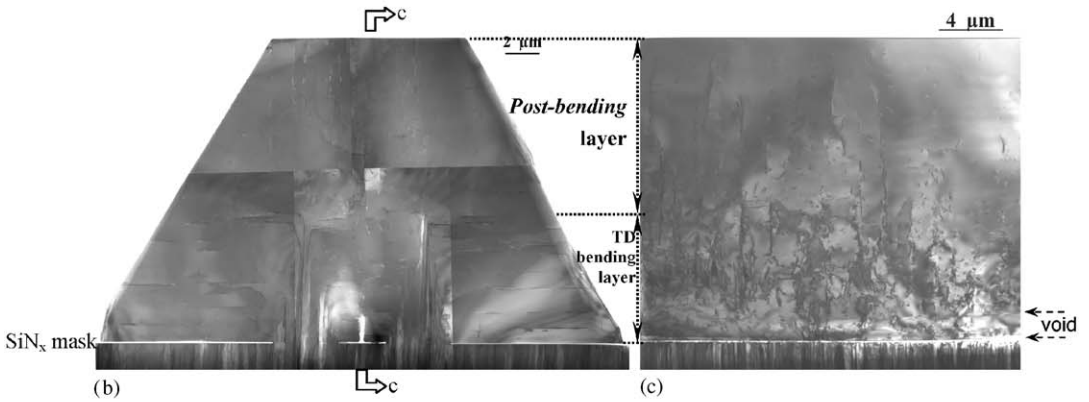
c
2 μm
Post-bending
layer
TD
bending
layer
SiNx mask
c
4 μm
void

(b) (c)

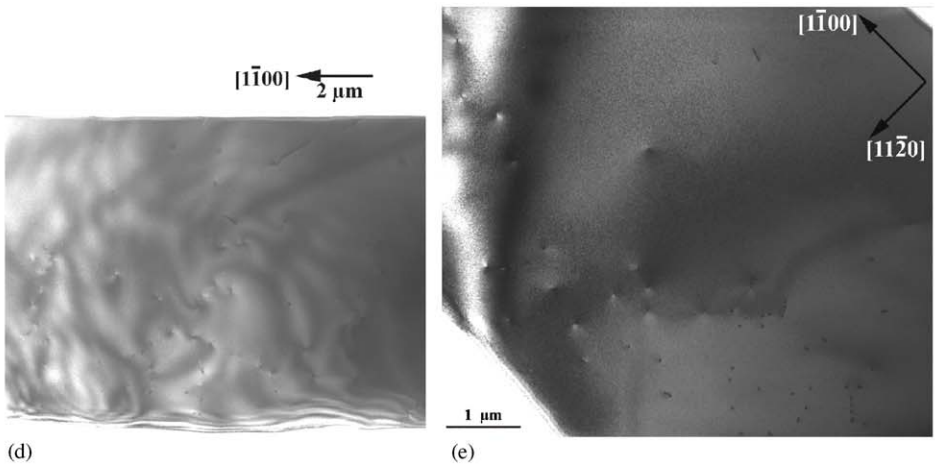
[1$\bar{1}$00]
2 μm
[1$\bar{1}$00]
[11$\bar{2}$0]
1 μm

(d) (e)

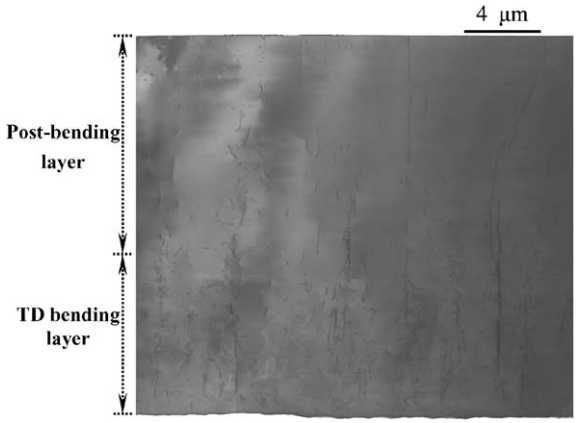

Fig. 2. Bright-field TEM image of another $(1\,1\,\bar{2}\,0)$ longitudinal cross-section under the $[1\,1\,\bar{2}\,0]$ zone axis without bending contours, since this piece of epi-layer cross-section has broken off from the SiN_x mask in the same piece of sample as that in Fig. 1(c).

piece of sample as that in Fig. 1(c). In Fig. 2, big coalescence misfit dislocations, which propagate into the post-bending layer, are discretely distributed with crooked lines with an average spacing of 6 μm. Determined from Fig. 2, the dislocation density in the post-bending layer is $\sim 8 \times 10^7\,cm^{-2}$, which is in good agreement with the estimation from Fig. 1(b). Detailed dislocation characterization will be presented in the next section.

3.2. Dislocation type characterization of GaN nonplanar substrate

The **g**∗**b** dark field analysis has been carried out to characterize dislocation variety distribution in the two sub-layers of the trapezoidal mesa substrate. Fig. 3(a) and (b) are the $g = (1\,1\,\bar{2}\,0)$ and $(0\,0\,0\,2)$ dark field TEM images of the transversal $(1\,\bar{1}\,0\,0)$ cross-section, corresponding to the center part of the TD bending layer. Many bending TDs are in contrast for both dark field images and therefore should be mixed **a**+**c** type dislocations with Burgers vector $\mathbf{b} = \frac{1}{3}\langle 1\,1\,\bar{2}\,3\rangle$. Several dislocations indicated by the letter "c" in Fig. 3(b), that are extinguished in the $(1\,1\,\bar{2}\,0)$ dark field, should be **c**-type dislocations with Burgers vector $\mathbf{b} = \langle 0\,0\,0\,1\rangle$. Other bending dislocations should be **a**-type dislocations with Burgers vector $\mathbf{b} = \frac{1}{3}\langle 1\,1\,\bar{2}\,0\rangle$ [indicated by the letter "a" in Fig. 3(a)], since they lose contrast or keep only residual contrast in the $\langle 0\,0\,0\,2\rangle$ dark field. As observed in this bending layer, the density of the **a**-type or mixed **a**+**c**-type dislocations is much higher than the **c** type dislocations.

The $\mathbf{g} = (1\,1\,\bar{2}\,0)$ and $(0\,0\,0\,2)$ dark field TEM images of the transversal $(1\,\bar{1}\,0\,0)$ cross-section are shown in Fig. 3(c) and (d), corresponding to the post-bending layer. There are many short RDs nearly vertical to the c top surface in the $(1\,1\,\bar{2}\,0)$ dark field. Almost all of them lose contrast in the $(0\,0\,0\,2)$ dark field Fig. 3(d) and hence should be **a** type dislocations with Burgers vector $\mathbf{b} = \frac{1}{3}\langle 1\,1\,\bar{2}\,0\rangle$. These dislocations are not as straight as the TDs in the bending layer. In Fig. 3(c), dashed lines appear in one or both ends of these **a** type dislocation lines while constant contrast is maintained in the center part of these dislocation lines, which shows that these dislocations propagate in the $\{1\,\bar{1}\,0\,0\}$ planes for a certain short length and then gradually slant outside the foil plane at either end. No loop is found here after the sample is tilted 30° around the $[1\,1\,\bar{2}\,0]$ or $[0\,0\,0\,1]$ axis. A few mixed **a**+**c** type dislocations seen in both dark field images, indicated by the letter "m" in Fig. 3(d), are located very close to the TD bending layer.

Similar dark field analysis is applied to characterizing dislocations existing in two sub-layers of the longitudinal cross-section. Fig. 4(a) and (b) are the $\mathbf{g} = (1\,\bar{2}\,1\,0)$ and $(0\,0\,0\,2)$ dark field TEM images corresponding to the lower TD bending layer. Edge-on dislocations observed in Fig. 4(a)

Fig. 1. Microstructures inside the GaN nonplanar substrate. (a) Sketch of mask design for nonplanar LEO GaN substrate, with different 3D view directions indicated corresponding to the following (b–e) bright-field TEM views; (b) $(1\,\bar{1}\,0\,0)$ transversal cross-section under the $[1\,\bar{1}\,0\,0]$ zone axis, which is composed of five micrographs collaged together, can be divided into a TD bending layer and a post-bending layer; (c) $(1\,1\,\bar{2}\,0)$ longitudinal cross-section under the $[1\,1\,\bar{2}\,0]$ zone axis is passing right through the center void of (b), with void trace pointed out by arrows; (d) plan-view image of the top most region of the mesa along the $[0\,0\,0\,1]$ zone axis; (e) an enlarged image of a part of (d).

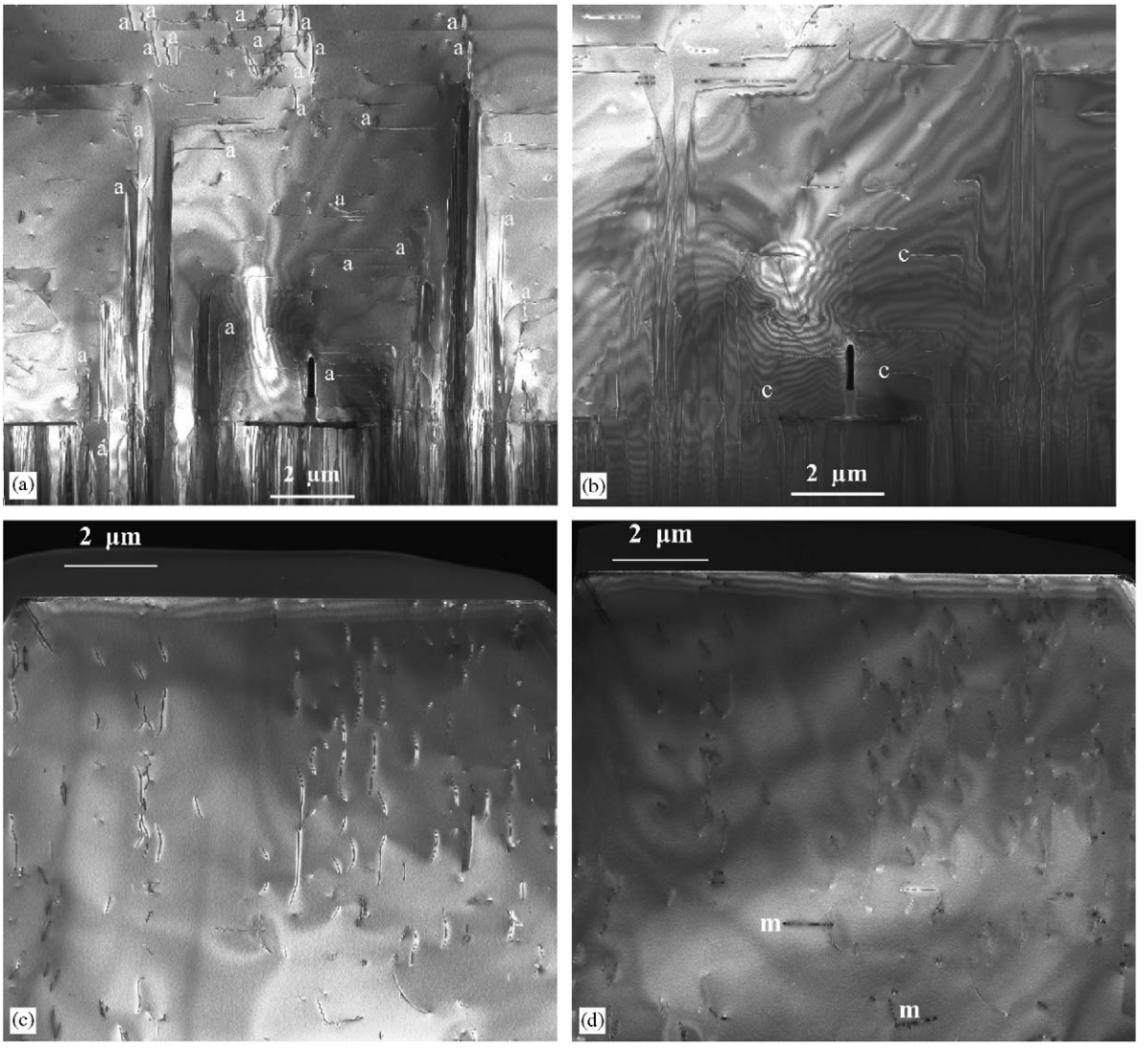

Fig. 3. Dark-field TEM images of the transversal cross-section of the LEO GaN nonplanar substrate near the $[1\,\bar{1}\,0\,0]$ zone axis. (a) $\mathbf{g} = (1\,1\,\bar{2}\,0)$ and (b) $\mathbf{g} = (0\,0\,0\,2)$ are corresponding to the center part of the TD bending layer. (c) $\mathbf{g} = (1\,1\,\bar{2}\,0)$ and (d) $\mathbf{g} = (0\,0\,0\,2)$ are dark-field images of the post-bending layer. Letter "a", "c" and "m" are respectively referred to the **a** type, **c** type and mixed **a** + **c** type dislocation.

are actually bent-over HDs. A few **c** type dislocations are observable in the TD bending layer with a low density of $\sim 10^6\,\mathrm{cm}^{-2}$. There exist a lot of **a** type dislocations [losing contrast in the (0 0 0 2) dark field] near the coalescence front, with a density of $\sim 2 \times 10^8\,\mathrm{cm}^{-2}$. Only those dislocations that stay in contrast in both conditions are mixed **a** + **c** type with a density of $\sim 3.5 \times 10^7\,\mathrm{cm}^{-2}$. These dislocations tend to entangle together and even form bigger coalescence dislocations. Fig. 4(c) and (d) are the $[1\,0\,\bar{1}\,0]$ bright field and $\mathbf{g} = (0\,0\,0\,2)$ dark field TEM images corresponding to the upper post-bending layer (near the mesa top). Most of dislocations are found to be out of contrast and

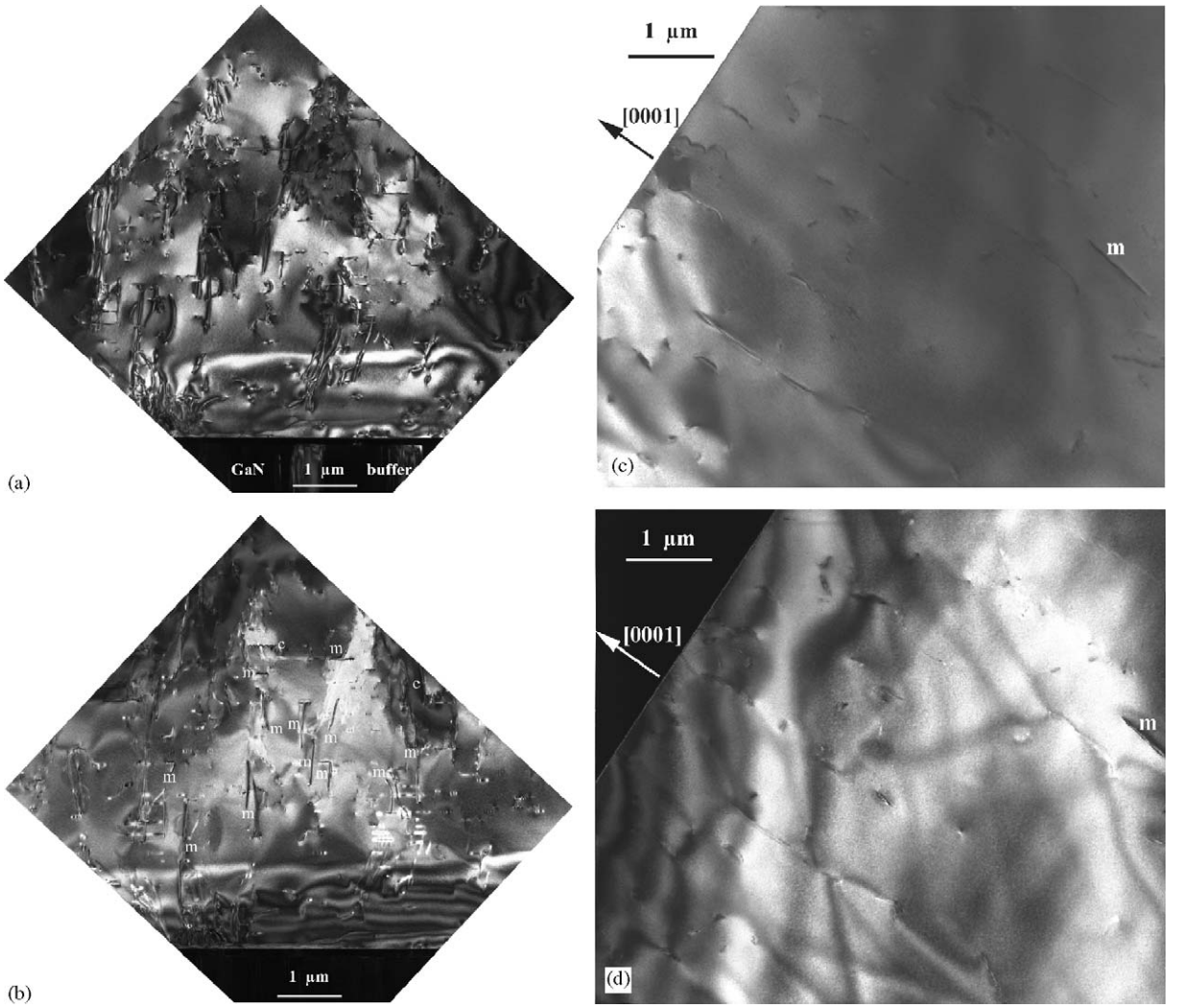

Fig. 4. Longitudinal cross-section TEM images of the LEO GaN nonplanar substrate near the $[1\,0\,\bar{1}\,0]$ zone axis. (a) $\mathbf{g} = (1\,\bar{2}\,1\,0)$ and (b) $\mathbf{g} = (0\,0\,0\,2)$ are dark-field images corresponding to the lower TD bending layer. (c) and (d) are the $[1\,0\,\bar{1}\,0]$ bright field and $\mathbf{g} = (0\,0\,0\,2)$ dark field TEM images of the upper post-bending layer (near the mesa top). Letter "c" and "m" designate the **c** type and mixed **a** + **c** type dislocations respectively.

hence should be **a** type with an estimated density of $\sim 8 \times 10^7\,\mathrm{cm}^{-2}$. A few **a** + **c** type dislocations are occasionally observed here.

In summary, the distributions of dislocations within two sub-layers of the nonplanar GaN LEO substrate are illustrated in the following Table 1. Dislocations that are capable of threatening our device performance mainly consist of **a** type dislocations with significant edge component.

3.3. Discussion

Figs. 5(a) and (b) are schematic drawings of the dislocation distribution in the LEO GaN nonplanar substrate, concluded from TEM observation. As illustrated in Fig. 5(b), after bending, TDs penetrating through mask windows propagate along a horizontal direction in the (0 0 0 1) basal plane. Some TDs adopt abrupt bending while

other TDs may propagate along a gradual changing route before entering the basal plane. As a result almost none of the TDs is able to reach the top plane after complete coalescence of both sub LEO stripes. One half of bent TD will propagate to the $\{1\,1\,\bar{2}\,2\}$ sidewall and terminate. But another half of those dislocations that bend towards coalescence front normally do not terminate at the center. Only those dislocations propagating close to the center void will run downward and terminate at the void. There are only **a**-type dislocations remaining in the post-bending layer, and no mixed **a**+**c** or **c** type dislocation near the mesa top.

Table 1
Dislocation distributions in the complete GaN nonplanar substrate (based on **g**∗**b** analysis results)

	Dislocation densities (cm^{-2}) corresponding to different types		
	a type $\mathbf{b}=\frac{1}{3}\langle 1\,1\,\bar{2}\,0\rangle$	**c** type $\mathbf{b}=\langle 0\,0\,0\,1\rangle$	Mixed **a**+**c** type $\mathbf{b}=\frac{1}{3}\langle 1\,1\,\bar{2}\,3\rangle$
Post-bending layer	8×10^{7}	~0	$\leqslant10^{6}$
TD bending layer	10^{9}	$\leqslant10^{6}$	10^{9}
Buffer layer	$\sim5\times10^{9}$	10^{7}	$\sim6\times10^{9}$

Fig. 5(a) shows that the chance of dislocation interaction is very high near the coalescence region in the TD bending layer. The above TEM results confirmed the intensive entangling of dislocations in the TD bending layer between the two mask windows. These evidences indicate that there are extensive interactions and reactions between the bent TDs in the TD bending layer between the windows since they are running head to head and easy to come within a reaction distance r_I of one another, where r_I can be equal to the dislocation annihilation radius r_A or the analogous dislocation fusion reaction radius r_F. TD's r_A was estimated to be 275 Å in GaN material [27].

According to the "$\mathbf{b}^2$-criterion", successful dislocation reactions should meet the requirement of film free energy minimization, that is $b_1^2+b_2^2\geqslant b_3^2$ [27]. The reactions between **a** type and **c** type dislocations, between **a**-type dislocations themselves and between **c**-type dislocations themselves

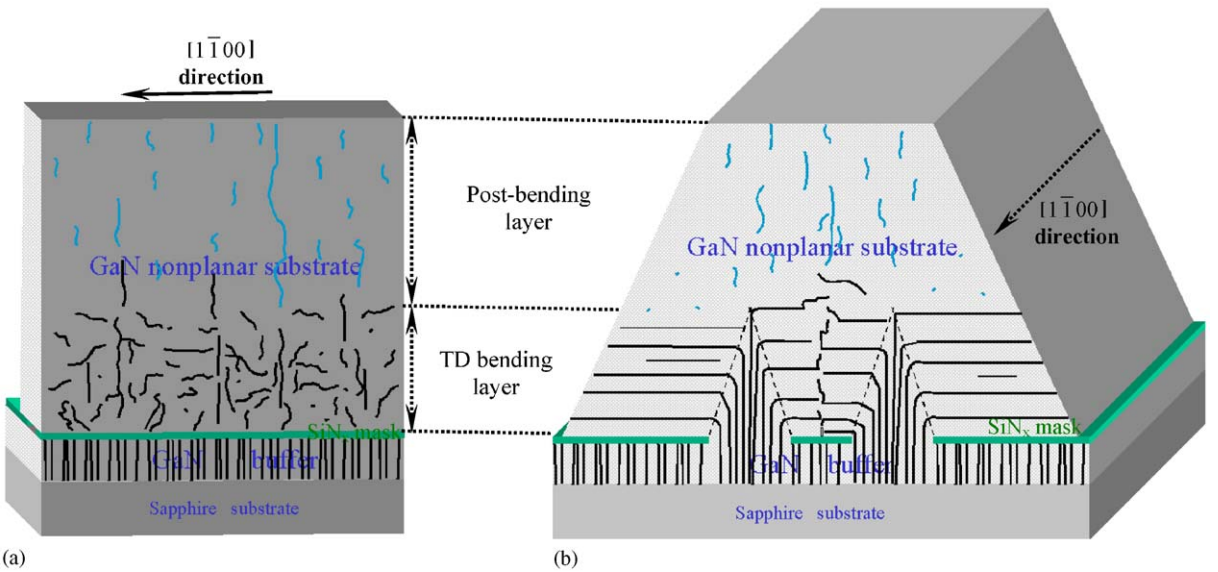

Fig. 5. Schematic drawing of dislocation distribution in the LEO GaN nonplanar substrate: black lines represent all kinds of dislocations while cyan lines represent **a** type dislocations only. (a) Sketch of the $(1\,1\,\bar{2}\,0)$ longitudinal cross-section cut along the stripe center of (b). (b) Sketch of the $(1\,\bar{1}\,0\,0)$ transversal cross-section for nonplanar GaN substrate.

are found impossible judged by this criterion. However, the participation of the mixed **a**+**c** type dislocation is inevitable for any possible dislocation reaction in GaN material, which depletes almost all of them. The possible byproducts of reactions between **a**+**c** type and **a**+**c** or **c**-type dislocations are pure **a** type dislocations. Although the byproducts of possible reactions between **a**+**c** type and **a** type dislocations are composed of **c** type and **a**+**c** type dislocations, these byproducts can react again to produce **a** type dislocations. Since mixed **a**+**c** type and **c** type dislocations are mostly consumed in the TD bending layer, the main remnant products of intensive reactions, **a** type dislocations, are able to propagate up into the post-bending layer to form the RDs. Thus it is not surprising at all to see that only pure **a** type dislocations remain when coming into the post-bending layer. The contribution from big misfit dislocations at the coalescence region is relatively small because of the low density of $3–4\times10^6\,\mathrm{cm}^{-2}$ verified in Fig. 2.

4. Summary

In summary, two-step LEO has been successfully carried out to attain coalesced low-defect-density nonplanar GaN substrate templates for high performance device fabrication. The tendency for TDs to bend 90° has been utilized to significantly prevent TDs from reaching the upper layer used for future device integration. The 3D distributions of different types of dislocations in the LEO nonplanar templates have been studied by TEM. Only pure **a** type dislocations with Burgers vector $\mathbf{b}=\frac{1}{3}\langle 1\,1\,\bar{2}\,0\rangle$ are found to remain in the upper post-bending layer with a density of $8\times10^7\,\mathrm{cm}^{-2}$. TEM study in the longitudinal cross-section has verified intensive entangling and reactions of dislocations in the TD bending layer between the two mask windows. Coalescence misfit dislocations with a low density of $3–4\times10^6\,\mathrm{cm}^{-2}$ are determined to be insufficient to invoke these **a**-type remnant dislocations. Reactions involving **a**+**c** type dislocations, which take place at the TD bending layer, are energetically preferable according to the dislocation line energy criterion, which also explains why no mixed **a**+**c** or **c** type dislocations is able to approach the template surface. Dislocation reaction mechanism is considered to play a crucial role in the dislocation reduction and **a**-type remnant dislocations formation in the post-bending layer.

Acknowledgments

This work is supported by DARPA. The authors are grateful to Dr. Edward Goo for fruitful discussion.

References

[1] Y.-F. Wu, B.P. Keller, P. Fini, S. Keller, T.J. Jenkins, L.T. Kehias, S.P. DenBaars, U.K. Mishra, IEEE Electron Device Lett. 19 (1998) 50.
[2] H. Morkoc, Nitride Semiconductors and Devices, Springer, Berlin, 1999.
[3] S. Nakamura, G. Fosol, The Blue Laser Diode, Springer, Berlin, 1998.
[4] R.F. Davis, S. Einfeldt, E.A. Preble, A.M. Roskowski, Z.J. Reitmeier, P.Q. Miraglia, Acta Mater. 51 (2003) 5961.
[5] F.A. Ponce, MRS Bull. Feb. 51 (1997).
[6] S. Keller, B.P. Keller, Y.F. Wu, B. Heying, D. Kapolnek, J.S. Speck, U.K. Mishra, S.P. DenBaars, Appl. Phys. Lett. 68 (1996) 1525.
[7] N.G. Weimann, L.F. Eastman, D. Dharanipal, H.M. Ng, T.D. Moustakas, J. Appl. Phys. 83 (1998) 3656.
[8] S. Nakamura, M. Senoh, S. Nagahama, N. Iwasa, T. Yamada, T. Matsushita, H. Kiyoku, Y. Sugimoto, T. Kozaki, H. Umemoto, M. Sano, K. Chocho, Jpn. J. Appl. Phys. Lett. 37 (1998) 309.
[9] H. Marchand, X.H. Wu, J.P. Ilbbetson, P.T. Fini, P. Kozodoy, S. Keller, J.S. Speck, S.P. DenBaars, U.K. Mishra, Appl. Phys. Lett. 73 (1998) 747.
[10] B. Beaumont, M. Vaille, G. Nataf, A. Bouillé, J.-C. Guillaume, P. Vennéguès, S. Haffouz, P. Gibart, MRS Internet J. Nitride Semicond. Res. 3 (1998) Art 20.
[11] P. Vennéguès, B. Beaumont, S. Haffouz, M. Vaille, P. Gibart, J. Crystal Growth 187 (1998) 167.
[12] A. Usui, H. Sunakawa, A. Sakai, A.A. Yamaguchi, Jpn. J. Appl. Phys. Lett. 36 (1997) 899.
[13] K. Hiramatsu, K. Nishiyama, M. Onishi, H. Mizutani, M. Narukawa, A. Motogaito, H. Miyake, Y. Iyechika, T. Maeda, J. Crystal Growth 221 (2000) 316.
[14] R.F. Davis, T. Gehrke, K.J. Linthicum, T.S. Zheleva, P. Rajagopal, E. Preble, C.A. Zorman, M. Mehregany, Proceedings of the International Workshop on Nitride Semiconductors IPAP Conference Series 1, 2000, pp. 267–271.

[15] S. Nitta, M. Kariya, T. Kashima, S. Yamaguchi, H. Amano, I. Akasaki, Appl. Surf. Sci. 159–160 (2000) 421.
[16] A. Sakai, H. Sunakawa, A. Kimura, A. Usui, Appl. Phys. Lett. 76 (2000) 442.
[17] K. Horibuchi, N. Kuwano, K. Oki, Y. Kawaguchi, N. Sawaki, K. Hiramatsu, Phys. Stat. Sol. A 180 (2000) 171.
[18] P. Vennéguès, B. Beaumont, V. Bousquet, M. Vaille, P. Gibart, J. Appl. Phys. 87 (2000) 4175.
[19] Hanmin Zhao, Yong Cheng, Michael.H. MacDougal, Gye-Mo. Yang, P.D. Dapkus, IEEE Photon. Technol. Lett. 7 (1995) 6.
[20] Dawei Ren, Wei Zhou, Xingang Zhang, P.D. Dapkus, D.H. Rich, InGaN/GaN buried heterostructures formed by MOCVD growth on non planar substrates, EMC 2003.
[21] B.P. Keller, S. Keller, D. Kapolnek, W.N. Jiang, Y.-F. Wu, H. Masui, X.H. Wu, B. Heying, J.S. Speck, U.K. Mishra, S.P. DenBaars, J. Electron. Mater. 24 (1992) 1707.
[22] D. Kapolnek, S. Keller, R. Vetury, R.D. Underwood, P. Kozodoy, S.P. Denbaars, U.K. Mishra, Appl. Phys. Lett. 71 (1997) 1204.
[23] G. Nataf, B. Beaumont, A. Bouillé, S. Haffouz, M. Vaille, P. Gibart, J. Crystal Growth 192 (1998) 73.
[24] Wei Zhou, Dawei Ren, P.D. Dapkus, Transmission electron microscopy study of defect reduction in two-step lateral epitaxial overgrown nonplanar GaN substrate, J. Crystal Growth, Submitted for publication.
[25] S.J. Klepeis, J.P. Benedict, R.M. Anderson, A Grinding/Polishing Tool for TEM Sample Preparation, Mater. Res. Soc. Proc. 115, Pittsburgh, PA USA, 179, 1987, 9
[26] Z. Liliental-Weber, M. Benamara, W. Swider, J. Washburn, J. Park, P.A. Grudowski, C.J. Eiting, R.D. Dupuis, MRS Internet J. Nitride Semicond. Res. 4s1 (1999) 4.6.
[27] S.K. Mathis, A.E. Romanov, L.F. Chen, G.E. Beltz, W. Pompe, J.S. Speck, J. Crystal Growth 231 (2001) 371.